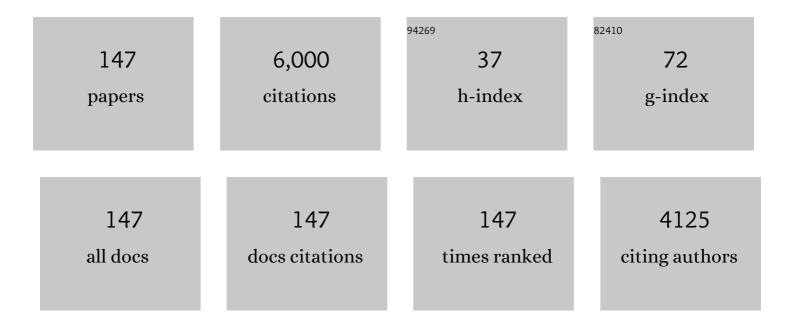
## Jin-Yoo Suh

List of Publications by Year in descending order

Source: https://exaly.com/author-pdf/8993904/publications.pdf Version: 2024-02-01



IN-YOO SUH

#	Article	IF	CITATIONS
1	Designing metallic glass matrix composites with high toughness and tensile ductility. Nature, 2008, 451, 1085-1089.	13.7	1,302
2	Development of tough, low-density titanium-based bulk metallic glass matrix composites with tensile ductility. Proceedings of the National Academy of Sciences of the United States of America, 2008, 105, 20136-20140.	3.3	308
3	Ferrite nucleation potency of non-metallic inclusions in medium carbon steels. Acta Materialia, 2001, 49, 2115-2122.	3.8	229
4	Microstructural evolutions of the Al strip prepared by cold rolling and continuous equal channel angular pressing. Acta Materialia, 2002, 50, 4005-4019.	3.8	189
5	Resistance of CoCrFeMnNi high-entropy alloy to gaseous hydrogen embrittlement. Scripta Materialia, 2017, 135, 54-58.	2.6	166
6	Spherical nanoindentation creep behavior of nanocrystalline and coarse-grained CoCrFeMnNi high-entropy alloys. Acta Materialia, 2016, 109, 314-322.	3.8	156
7	Indentation size effect and shear transformation zone size in a bulk metallic glass in two different structural states. Acta Materialia, 2012, 60, 6862-6868.	3.8	130
8	Finite element analysis of material flow in equal channel angular pressing. Scripta Materialia, 2001, 44, 677-681.	2.6	122
9	Strengthening mechanism of hot rolled Ti and Nb microalloyed HSLA steels containing Mo and W with various coiling temperature. Materials Science & Engineering A: Structural Materials: Properties, Microstructure and Processing, 2013, 560, 528-534.	2.6	110
10	Nanomechanical behavior and structural stability of a nanocrystalline CoCrFeNiMn high-entropy alloy processed by high-pressure torsion. Journal of Materials Research, 2015, 30, 2804-2815.	1.2	101
11	The role of hydrogen in hardening/softening steel: Influence of the charging process. Scripta Materialia, 2015, 107, 46-49.	2.6	99
12	Estimation of the shear transformation zone size in a bulk metallic glass through statistical analysis of the first pop-in stresses during spherical nanoindentation. Scripta Materialia, 2012, 66, 923-926.	2.6	92
13	Microstructure and mechanical properties of friction stir welded and laser welded high entropy alloy CrMnFeCoNi. Metals and Materials International, 2018, 24, 73-83.	1.8	84
14	Inoculated acicular ferrite microstructure and mechanical properties. Materials Science & Engineering A: Structural Materials: Properties, Microstructure and Processing, 2001, 319-321, 326-331.	2.6	82
15	Development of lightweight Mg Li Al alloys with high specific strength. Journal of Alloys and Compounds, 2016, 680, 116-120.	2.8	82
16	Effect of die shape on the deformation behavior in equal-channel angular pressing. Metallurgical and Materials Transactions A: Physical Metallurgy and Materials Science, 2001, 32, 3007-3014.	1.1	77
17	Fracture toughness and crack-resistance curve behavior in metallic glass-matrix composites. Applied Physics Letters, 2009, 94, .	1.5	64
18	Annealing effect on plastic flow in nanocrystalline CoCrFeMnNi high-entropy alloy: A nanomechanical analysis. Acta Materialia, 2017, 140, 443-451.	3.8	61

#	Article	IF	CITATIONS
19	Molecular dynamics simulation of the crystallization of a liquid gold nanoparticle. Journal of Crystal Growth, 2003, 250, 558-564.	0.7	52
20	Correlation between fracture surface morphology and toughness in Zr-based bulk metallic glasses. Journal of Materials Research, 2010, 25, 982-990.	1.2	52
21	Influence of Zr content on phase formation, transition and mechanical behavior of Ni-Ti-Hf-Zr high temperature shape memory alloys. Journal of Alloys and Compounds, 2017, 692, 77-85.	2.8	52
22	Fracture toughness study of new Zr-based Be-bearing bulk metallic glasses. Scripta Materialia, 2009, 60, 80-83.	2.6	50
23	High-temperature creep behavior and microstructural evolution of an 18Cr9Ni3CuNbVN austenitic stainless steel. Materials Characterization, 2014, 93, 52-61.	1.9	50
24	Glassy steel optimized for glass-forming ability and toughness. Applied Physics Letters, 2009, 95, .	1.5	49
25	Structural evolution of a strip-cast al alloy sheet processed by continuous equal-channel angular pressing. Metallurgical and Materials Transactions A: Physical Metallurgy and Materials Science, 2002, 33, 665-673.	1.1	48
26	Enhanced Desorption and Absorption Properties of Eutectic LiBH <sub>4</sub> –Ca(BH <sub>4</sub> ) <sub>2</sub> Infiltrated into Mesoporous Carbon. Journal of Physical Chemistry C, 2011, 115, 20027-20035.	1.5	48
27	High-temperature tensile and creep deformation of cross-weld specimens of weld joint between T92 martensitic and Super304H austenitic steels. Materials Characterization, 2014, 97, 161-168.	1.9	47
28	Effective thermal conductivity of MgH2 compacts containing expanded natural graphite under a hydrogen atmosphere. International Journal of Hydrogen Energy, 2014, 39, 349-355.	3.8	47
29	Micro-to-nano-scale deformation mechanisms of a bimodal ultrafine eutectic composite. Scientific Reports, 2014, 4, 6500.	1.6	46
30	Gradual martensitic transformation of B2 phase on TiCu-based bulk metallic glass composite during deformation. Intermetallics, 2016, 75, 1-7.	1.8	45
31	Deformation mechanisms and texture evolution in high entropy alloy during cold rolling. International Journal of Plasticity, 2021, 141, 102989.	4.1	45
32	Metal halide doped metal borohydrides for hydrogen storage: The case of Ca(BH4)2–CaX2 (X=F, Cl) mixture. Journal of Alloys and Compounds, 2010, 506, 721-727.	2.8	44
33	Numerical simulation of long-term precipitate evolution in austenitic heat-resistant steels. Calphad: Computer Coupling of Phase Diagrams and Thermochemistry, 2010, 34, 105-112.	0.7	44
34	Effect of aging treatment on microstructure and intrinsic mechanical behavior of Fe–31.4Mn–11.4Al–0.89C lightweight steel. Journal of Alloys and Compounds, 2016, 656, 805-811.	2.8	44
35	New processing possibilities for highly toughened metallic glass matrix composites with tensile ductility. Scripta Materialia, 2008, 59, 684-687.	2.6	41
36	Influence of pre-strain on the gaseous hydrogen embrittlement resistance of a high-entropy alloy. Materials Science & Engineering A: Structural Materials: Properties, Microstructure and Processing, 2018, 718, 43-47.	2.6	41

#	Article	IF	CITATIONS
37	Influences of hydrogen charging method on the hydrogen distribution and nanomechanical properties of face-centered cubic high-entropy alloy: A comparative study. Scripta Materialia, 2019, 168, 76-80.	2.6	39
38	Work-hardening and plastic deformation behavior of Ti-based bulk metallic glass composites with bimodal sized B2 particles. Intermetallics, 2015, 62, 36-42.	1.8	38
39	Nano-graining a particle-strengthened high-entropy alloy. Scripta Materialia, 2019, 163, 24-28.	2.6	38
40	Enhancing the Hydrogen Storage Properties of AxBy Intermetallic Compounds by Partial Substitution: A Short Review. Hydrogen, 2020, 1, 38-63.	1.7	38
41	Effect of hydrogen on the yielding behavior and shear transformation zone volume in metallic glass ribbons. Acta Materialia, 2014, 78, 213-221.	3.8	36
42	Evaluation of formability and planar anisotropy based on textures in aluminum alloys processed by a shear deforming process. Materials Science & Engineering A: Structural Materials: Properties, Microstructure and Processing, 2008, 477, 107-120.	2.6	35
43	Rehydrogenation and cycle studies of LiBH4–CaH2 composite. International Journal of Hydrogen Energy, 2010, 35, 6578-6582.	3.8	35
44	Hydrogen-induced nanohardness variations in a CoCrFeMnNi high-entropy alloy. International Journal of Hydrogen Energy, 2017, 42, 12015-12021.	3.8	35
45	Effect of post-weld heat treatment on the microstructure and hardness of P92 steel in IN740H/P92 dissimilar weld joints. Materials Characterization, 2020, 160, 110083.	1.9	35
46	Effect of deformation histories on texture evolution during equal- and dissimilar-channel angular pressing. Scripta Materialia, 2003, 49, 185-190.	2.6	34
47	Metastable hexagonal close-packed palladium hydride in liquid cell TEM. Nature, 2022, 603, 631-636.	13.7	31
48	Hydrogen-induced hardening and softening of Ni–Nb–Zr amorphous alloys: Dependence on the Zr content. Scripta Materialia, 2014, 93, 56-59.	2.6	30
49	Unraveling the origin of strain-induced precipitation of M23C6 in the plastically deformed 347 Austenite stainless steel. Materials Characterization, 2014, 94, 7-13.	1.9	30
50	Influence of hydrogen on incipient plasticity in CoCrFeMnNi high-entropy alloy. Scripta Materialia, 2019, 161, 23-27.	2.6	30
51	Development of nano-crystalline cold sprayed Ni–20Cr coatings for high temperature oxidation resistance. Surface and Coatings Technology, 2015, 266, 122-133.	2.2	29
52	Magnesium- and intermetallic alloys-based hydrides for energy storage: modelling, synthesis and properties. Progress in Energy, 2022, 4, 032007.	4.6	29
53	Kinetics and thermodynamics of near eutectic Mg-Mg2Ni composites produced by casting process. International Journal of Hydrogen Energy, 2020, 45, 29009-29022.	3.8	28
54	Combinatorial Influence of Bimodal Size of B2 TiCu Compounds on Plasticity of Ti-Cu-Ni-Zr-Sn-Si Bulk Metallic Glass Composites. Metallurgical and Materials Transactions A: Physical Metallurgy and Materials Science, 2014, 45, 2376-2381.	1.1	27

#	Article	IF	CITATIONS
55	Microstructural evolution and creep-rupture life estimation of high-Cr martensitic heat-resistant steels. Materials Characterization, 2015, 106, 266-272.	1.9	27
56	Role of alloying elements in vanadium-based binary alloy membranes for hydrogen separation. Journal of Membrane Science, 2012, 423-424, 332-341.	4.1	26
57	Role of Hydrogen and Temperature in Hydrogen Embrittlement of Equimolar CoCrFeMnNi High-entropy Alloy. Metals and Materials International, 2021, 27, 166-174.	1.8	26
58	Direct measurement of hydrogen diffusivity through Pd-coated Ni-based amorphous metallic membranes. Journal of Membrane Science, 2013, 436, 195-201.	4.1	25
59	Hydrogen embrittlement in high interstitial alloyed 18Cr10Mn austenitic stainless steels. International Journal of Hydrogen Energy, 2015, 40, 13635-13642.	3.8	25
60	Enhanced high temperature hydrogen permeation characteristics of V–Ni alloy membranes containing a trace amount of yttrium. Scripta Materialia, 2016, 116, 122-126.	2.6	25
61	Hydrogen Back-Pressure Effects on the Dehydrogenation Reactions of Ca(BH <sub>4</sub> ) <sub>2</sub> . Journal of Physical Chemistry C, 2012, 116, 25715-25720.	1.5	24
62	Prediction of hydrogen permeability in V–Al and V–Ni alloys. Journal of Membrane Science, 2013, 430, 234-241.	4.1	24
63	Development of high strength hot rolled low carbon copper-bearing steel containing nanometer sized carbides. Materials Science & Engineering A: Structural Materials: Properties, Microstructure and Processing, 2015, 633, 1-8.	2.6	24
64	Influence of microstructural evolution on mechanical behavior of Fe–Nb–B ultrafine composites with a correlation to elastic modulus and hardness. Journal of Alloys and Compounds, 2015, 647, 886-891.	2.8	24
65	Deformation mechanisms to ameliorate the mechanical properties of novel TRIP/TWIP Co-Cr-Mo-(Cu) ultrafine eutectic alloys. Scientific Reports, 2017, 7, 39959.	1.6	24
66	Chemical heterogeneity-induced plasticity in Ti–Fe–Bi ultrafine eutectic alloys. Materials & Design, 2014, 60, 363-367.	5.1	23
67	Tailoring the equilibrium hydrogen pressure of TiFe via vanadium substitution. Journal of Alloys and Compounds, 2021, 854, 157263.	2.8	23
68	Effect of Cr addition on room temperature hydrogenation of TiFe alloys. International Journal of Hydrogen Energy, 2021, 46, 19478-19485.	3.8	23
69	Effect of Nb addition on Z-phase formation and creep strength in high-Cr martensitic heat-resistant steels. Materials Characterization, 2015, 102, 79-84.	1.9	22
70	Synthesis of Mg2FeH6 by hydrogenation of Mg/Fe powder mixture prepared by cold roll milling in air: Effects of microstructure and oxygen distribution. International Journal of Hydrogen Energy, 2018, 43, 16758-16765.	3.8	22
71	Effect of gaseous hydrogen embrittlement on the mechanical properties of additively manufactured CrMnFeCoNi high-entropy alloy strengthened by in-situ formed oxide. Materials Science & Engineering A: Structural Materials: Properties, Microstructure and Processing, 2020, 796, 140039.	2.6	22
72	Hydrogen storage behavior and microstructural feature of a TiFe–ZrCr2 alloy. Journal of Alloys and Compounds, 2021, 853, 157099.	2.8	22

#	Article	IF	CITATIONS
73	Low temperature formation of Mg 2 FeH 6 by hydrogenation of ball-milled nano-crystalline powder mixture of Mg and Fe. Materials and Design, 2017, 135, 239-245.	3.3	21
74	An investigation of the microstructural effects on the mechanical and electrochemical properties of a friction stir processed equiatomic CrMnFeCoNi high entropy alloy. Journal of Materials Science and Technology, 2021, 87, 60-73.	5.6	21
75	Effect of vanadium addition on the creep resistance of 18Cr9Ni3CuNbN austenitic stainless heat resistant steel. Journal of Alloys and Compounds, 2013, 574, 532-538.	2.8	20
76	Long-term evolution of $\ddot{l}f$ phase in 304H austenitic stainless steel: Experimental and computational investigation. Materials Characterization, 2017, 128, 23-29.	1.9	20
77	Low-temperature tensile and impact properties of hydrogen-charged high-manganese steel. International Journal of Hydrogen Energy, 2019, 44, 7000-7013.	3.8	20
78	Hydrogen uptake and its influence in selective laser melted austenitic stainless steel: A nanoindentation study. Scripta Materialia, 2021, 194, 113718.	2.6	20
79	Activation of Ti–Fe–Cr alloys containing identical AB2 fractions. Journal of Alloys and Compounds, 2021, 864, 158876.	2.8	20
80	On the Formation and the Structure of the First Bimetallic Borohydride Borate, LiCa <sub>3</sub> (BH <sub>4</sub> )(BO <sub>3</sub> ) <sub>2</sub> . Journal of Physical Chemistry C, 2011, 115, 10298-10304.	1.5	19
81	Thermodynamics of the dehydrogenation of the LiBH4–YH3 composite: Experimental and theoretical studies. Journal of Alloys and Compounds, 2012, 510, L9-L12.	2.8	19
82	Design of sustainable V-based hydrogen separation membranes based on grain boundary segregation. International Journal of Hydrogen Energy, 2014, 39, 12031-12044.	3.8	19
83	Effect of Ca addition on the plastic deformation behavior of extruded Mg-11Li-3Al-1Sn-0.4Mn alloy. Journal of Alloys and Compounds, 2016, 687, 821-826.	2.8	19
84	Improved Creep Behavior of a High Nitrogen Nb-Stabilized 15Cr-15Ni Austenitic Stainless Steel Strengthened by Multiple Nanoprecipitates. Metallurgical and Materials Transactions A: Physical Metallurgy and Materials Science, 2011, 42, 3378-3385.	1.1	16
85	Hydrogen permeation characteristics of rolled V85Al10Co5 alloys. Current Applied Physics, 2012, 12, 1131-1138.	1.1	15
86	Effect of preexisting plastic deformation on the creep behavior of TP347 austenitic steel. Materials Science & Engineering A: Structural Materials: Properties, Microstructure and Processing, 2016, 654, 390-399.	2.6	15
87	Understanding first cycle hydrogenation properties of Ti–Fe–Zr ternary alloys. International Journal of Hydrogen Energy, 2021, 46, 4241-4251.	3.8	15
88	Effects of the deformation history and the initial textures on the texture evolution in an Al alloy strip during the shear deforming process. Acta Materialia, 2004, 52, 4907-4918.	3.8	14
89	Nanoscale light element identification using machine learning aided STEM-EDS. Scientific Reports, 2020, 10, 13699.	1.6	14
90	High temperature tensile and creep properties of CrMnFeCoNi and CrFeCoNi high-entropy alloys. Materials Science & Engineering A: Structural Materials: Properties, Microstructure and Processing, 2022, 838, 142748.	2.6	14

#	Article	IF	CITATIONS
91	Analysis on the phase transition behavior of Cu base bulk metallic glass by electrical resistivity measurement. Materials Science & Engineering A: Structural Materials: Properties, Microstructure and Processing, 2007, 449-451, 521-525.	2.6	13
92	The role of Fe particle size and oxide distribution on the hydrogenation properties of ball-milled nano-crystalline powder mixtures of Fe and Mg. Journal of Alloys and Compounds, 2019, 806, 1039-1046.	2.8	13
93	Hydrogen-induced decomposition of Cu–Zr binary amorphous metallic alloys. Journal of Alloys and Compounds, 2016, 660, 456-460.	2.8	12
94	Tensile and fracture behaviors of austenitic high-manganese steels subject to different hydrogen embrittlement test methods. Materials Science & Engineering A: Structural Materials: Properties, Microstructure and Processing, 2019, 766, 138367.	2.6	12
95	Exploring the hydrogen absorption and strengthening behavior in nanocrystalline face-centered cubic high-entropy alloys. Scripta Materialia, 2021, 203, 114069.	2.6	12
96	Novel thermoplastic bonding using a bulk metallic glass solder. Scripta Materialia, 2008, 59, 905-908.	2.6	11
97	Effect of Nb and Cu on the high temperature creep properties of a high Mn–N austenitic stainless steel. Materials Characterization, 2013, 83, 49-57.	1.9	11
98	Hydrogen-induced softening in nanocrystalline Ni investigated by nanoindentation. Philosophical Magazine, 2016, 96, 3442-3450.	0.7	11
99	Influence of Nb on microstructure and mechanical properties of Ti-Sn ultrafine eutectic alloy. Metals and Materials International, 2017, 23, 20-25.	1.8	11
100	A finite outlet volume correction to the time lag method: The case of hydrogen permeation through V-alloy and Pd membranes. Journal of Membrane Science, 2019, 585, 253-259.	4.1	11
101	Comparative Study of Hydrogen Embrittlement of Three Heat-resistant Cr-Mo Steels Subjected to Electrochemical and Gaseous Hydrogen Charging. Metallurgical and Materials Transactions A: Physical Metallurgy and Materials Science, 2020, 51, 2118-2125.	1.1	11
102	Effect of creep deformation on the microstructural evolution of 11CrMoVNb heat resistant steel. Materials Science & Engineering A: Structural Materials: Properties, Microstructure and Processing, 2012, 536, 92-97.	2.6	10
103	Atomistic simulation of hydrogen diffusion at tilt grain boundaries in vanadium. Metals and Materials International, 2013, 19, 1221-1225.	1.8	10
104	Properties of a rare earth free L10-FeNi hard magnet developed through annealing of FeNiPC amorphous ribbons. Current Applied Physics, 2019, 19, 599-605.	1.1	10
105	On the long-term cyclic stability of near-eutectic Mg–Mg2Ni alloys. International Journal of Hydrogen Energy, 2022, 47, 3939-3947.	3.8	10
106	CALPHAD-based alloy design for advanced automotive steels - Part I: Development of bearing steels with enhanced strength and optimized microstructure. Calphad: Computer Coupling of Phase Diagrams and Thermochemistry, 2016, 54, 165-171.	0.7	9
107	Flaw-Containing Alumina Hollow Nanostructures Have Ultrahigh Fracture Strength To Be Incorporated into High-Efficiency GaN Light-Emitting Diodes. Nano Letters, 2018, 18, 1323-1330.	4.5	9
108	Formation of needle-like MC carbide at or near incoherent twin boundary in IN740H Ni-based superalloy. Journal of Alloys and Compounds, 2020, 813, 152222.	2.8	9

#	Article	IF	CITATIONS
109	Microstructural evolution of P92 steel in IN740H/P92 dissimilar weld joints during creep deformation. Materials Science & Engineering A: Structural Materials: Properties, Microstructure and Processing, 2021, 821, 141614.	2.6	9
110	Deciphering the role of multiple generations of annealing twins on texture evolution in cold-rolled high entropy alloys during annealing. Scripta Materialia, 2021, 205, 114221.	2.6	9
111	Controlling the textures of the Al alloy sheet via dissimilar channel angular pressing. Materials Science & Engineering A: Structural Materials: Properties, Microstructure and Processing, 2005, 394, 60-65.	2.6	8
112	Hydrogen permeability of glass-forming Ni-Nb-Zr-Ta crystalline membranes. Metals and Materials International, 2011, 17, 541-545.	1.8	8
113	Nanometer-scale phase separation and formation of delta ZrH2 in Cu-Zr binary amorphous alloys. Journal of Alloys and Compounds, 2017, 721, 646-652.	2.8	8
114	Determining the effect of added zirconium on the bond character in TiFe alloys using scanning Kelvin probe force microscopy. Applied Surface Science, 2020, 517, 146163.	3.1	8
115	Heterogeneities in the microstructure and mechanical properties of high-Cr martensitic stainless steel produced by repetitive hot roll bonding. Materials Science & Engineering A: Structural Materials: Properties, Microstructure and Processing, 2021, 801, 140416.	2.6	8
116	Hydrogen occupation in Ti4M2O compounds (M = Fe, Co, Ni, Cu, and yÂ=Â0, 1) and their hydrogen storage characteristics. Journal of Alloys and Compounds, 2022, 891, 162050.	2.8	8
117	Self-healing behavior of Inconel 617B superalloy. Journal of Alloys and Compounds, 2019, 805, 1217-1223.	2.8	7
118	Nanomechanical and microstructural characterization on the synergetic strengthening in selectively laser melted austenitic stainless steel. Scripta Materialia, 2022, 209, 114359.	2.6	7
119	Micro-forming and surface evaluation of Zr41Ti14Cu12.5Ni10Be22.5 bulk metallic glass. Materials Science & Engineering A: Structural Materials: Properties, Microstructure and Processing, 2007, 454-455, 14-18.	2.6	6
120	Further evidence for room temperature, indentation-induced nanocrystallization in a bulk metallic glass. Materials Science & Engineering A: Structural Materials: Properties, Microstructure and Processing, 2012, 545, 225-228.	2.6	6
121	Magnetically soft FeCoTiZrB alloys with high saturation magnetization. Intermetallics, 2017, 90, 164-168.	1.8	6
122	Electrically Assisted Solid-State Joining of CrMnFeCoNi High-Entropy Alloy. Metallurgical and Materials Transactions A: Physical Metallurgy and Materials Science, 2020, 51, 6142-6148.	1.1	6
123	Design of V-Substituted TiFe-Based Alloy for Target Pressure Range and Easy Activation. Materials, 2021, 14, 4829.	1.3	6
124	Prediction of elastic properties of precipitation-hardened aluminum cast alloys. Computational Materials Science, 2012, 51, 365-371.	1.4	5
125	Mechanism for H-shaped precipitate formation in 1.25Cr-0.5Mo steel. Materials Characterization, 2020, 163, 110314.	1.9	5
126	Effect of Co on the degradation of the hydrogen permeability of Ni-Nb-Zr amorphous membranes. Metals and Materials International, 2014, 20, 215-219.	1.8	4

#	Article	IF	CITATIONS
127	<i>In Situ</i> Scanning Electron Microscopy Analysis of the Interfacial Failure of Oxide Scales on Stainless Steels and Its Effect on Sticking during Hot Rolling. ACS Omega, 2022, 7, 15174-15185.	1.6	4
128	Influence of Hydrogen Absorption on Stacking Fault of Energy of a Face-Centered Cubic High Entropy Alloy. Metals and Materials International, 2022, 28, 2637-2645.	1.8	4
129	A semi-empirical methodology to predict hydrogen permeability in amorphous alloy membranes. Journal of Membrane Science, 2014, 472, 102-109.	4.1	3
130	Reassessing the atomic size effect on glass forming ability: Effect of atomic size difference on thermodynamics and kinetics. Intermetallics, 2016, 69, 123-127.	1.8	3
131	EBSD microstructural analysis of AB-type TiFe hydrogen storage alloys. Materials Characterization, 2021, 178, 111276.	1.9	3
132	Orientation Rotation Behavior in Aluminum Alloys during Dissimilar Channel Angular Pressing. Materials Transactions, 2004, 45, 125-130.	0.4	2
133	Hydrogen Permeation Properties of Pd-Coated Ni <sub>37.5</sub> Nb <sub>27.5</sub> Zr <sub>25</sub> Co <sub>5</sub> Ta <sub>5</sub> Amorphous Membrane. Materials Science Forum, 2010, 654-656, 2823-2826.	0.3	2
134	Phase transformation and mechanical properties of as-cast Ti41.5Zr41.5Ni17 quasicrystalline composites. Journal of Non-Crystalline Solids, 2014, 392-393, 6-10.	1.5	2
135	Enhancement of mechanical properties in a Fe81Nb9B10 ultrafine-eutectic composite with in-situ polygonal pro-eutectic and encapsulating eutectic structure. Journal of Alloys and Compounds, 2015, 643, S204-S208.	2.8	2
136	Effect of Thermal Charging of Hydrogen on the Microstructure of Metastable Austenitic Stainless Steel. Steel Research International, 2017, 88, 1600063.	1.0	2
137	Hydrogen-induced change in microstructure and properties of steels: 18Cr10Mn–0.4N vis-Ã-vis 18Cr10Ni. Materials Science and Technology, 2018, 34, 584-586.	0.8	2
138	Microstructural Analysis of Dehydrogenation Products of the Ca(BH <sub>4</sub> ) <sub>2</sub> –MgH <sub>2</sub> Composite. Microscopy and Microanalysis, 2013, 19, 149-151.	0.2	1
139	Phase dependent magnetic properties of Ni–Au alloy nanowires. Materials Letters, 2014, 116, 86-90.	1.3	1
140	Structural homogeneity and mass density of bulk metallic glasses revealed by their rough surfaces and ultra-small angle neutron scattering (USANS). Scientific Reports, 2018, 8, 12986.	1.6	1
141	Microstructural investigation on the failure in APMT/KHR45A dissimilar weld interface after long-term service at high temperature. Materials Characterization, 2021, 176, 111110.	1.9	1
142	Processing Map for Zr-based In-situ β Phase Composites. Materials Research Society Symposia Proceedings, 2007, 1048, 5.	0.1	0
143	Fracture Toughness Study on Zr-based Bulk Metallic Glasses. Materials Research Society Symposia Proceedings, 2007, 1048, 4.	0.1	0
144	Thermodynamics and sorption reaction of some light metal borohydrides for reversible hydrogen storage. , 2010, , .		0

#	Article	IF	CITATIONS
145	Hydrogen permeation properties of in-situ Ti-based bulk metallic glass matrix composite membranes. , 2011, , .		0
146	Unusual flow behavior of Fe-based soft magnetic amorphous ribbons under high temperature tensile loading. Current Applied Physics, 2018, 18, 411-416.	1.1	0
147	Enhanced Hard-magnetic Properties of Rare Earth-free L1 <sub>0</sub> -FeNi Phase in FeNiPC Alloys. Journal of Magnetics, 2021, 26, 394-400.	0.2	0